ELSEVIER

JACEE Symposium

Nuclear Physics B (Proc. Suppl.) 60B (1998) 83–92

NUCLEAR PHYSICS B
PROCEEDINGS
SUPPLEMENTS

Elemental Abundance of High Energy Cosmic Rays

Yoshiyuki Takahashi

(for the JACEE Collaboration*)
Department of Physics,
The University of Alabama in Huntsville, Huntsville, AL35899, USA

Very high energy spectra of cosmic ray nuclei from the JACEE balloon experiments are presented. From a total of 12 balloon flights with an exposure factor of about 580 m^2 hour the energy spectra of nuclei have been obtained in the energy range from several TeV to 1,000 TeV. Proton energy spectrum, extending to several hundred TeV, can be a single-power law. Helium shows a single power law spectrum in the energy range from 2 TeV/n to 200 TeV/n. Other nuclei up to Fe indicated harder spectral indices compared with those of protons and helium. The composition at around 500 TeV is 16 ± 5%: 29 ± 5%: 35 ± 5%: 9 ± 3%: 11 ± 4%, for the abundance of p : He : C ~ O : Ne ~ S : Z ≥ 18.

1. INTRODUCTION

The origin of cosmic rays has been a question for many decades, and it still is a fundamental, astrophysical mystery.

Observed cosmic rays are composed of elements similar to the solar-abundance, except for secondary nuclei (e.g., light nuclei and sub-iron nuclei), trans-actinides, and some isotopes. Low energy cosmic rays (100 MeV/n - 100 GeV/n) were relatively well measured by various spacecraft experiments [1]. Models and theories to understand the energy spectra and elemental abundance of nuclei, as well as the propagation effects, have considerably been developed in the last few decades. Nevertheless, the very nature of cosmic rays beyond the shock limit ($E \geq 10^{14}$ eV) remains unclear. Presumably, drastic transition of the rigidity dependent elemental abundance is expected at these energies and is a good test for any models.

The standard model, generally accepted in the low energy region, is the Leaky-Box (LB) model [2], which considers interstellar shock acceleration of source materials and the diffusive propagation in a confinement volume with the rigidity-dependent escape length, $\lambda_{esc} \sim E^{-0.3}$, although its effective rigidity dependence up to about 100 GeV/n is approximately $\lambda_{esc} \sim E^{-0.6}$). The LB successfully explains gradual steepening of the energy spectra of nuclei ($\sim E^{-2.0} \rightarrow E^{-2.6}$)

*The JACEE Collaboration: K. Asakimori,[4] T.H. Burnett,[12] M.L. Cherry,[10] K. Chevli,[9] M.J. Christl,[11] S. Dake,[3] J.H. Derrickson,[11] W.F. Fountain,[11] M. Fuki,[5] J.C. Gregory,[9] R. Holynski,[13] J. Iwai,[12] A. Iyono,[7] W.V. Jones,[10] A. Jurak,[13] M. Kobayashi,[6] J.J. Lord,[12] O. Miyamura,[2] H. Oda,[3] T. Ogata,[1] E.D. Olson,[12] T.A. Parnell,[11] F.E. Roberts,[11] T. Shiina,[9] S.C. Strausz,[12] Y. Takahashi,[9] T. Tominaga,[9] S. Toyoda,[1] J.W. Watts,[11] Wefel,[10] B. Wilczynka,[13] H. Wilczynski,[13] R.J. Wilkes,[12] W. Wolter,[13] B. Wosiek,[13] H. Yokomi,[8] E.L. Zager.[12] *Univ. Tokyo,[1] Hiroshima Univ.,[2] Kobe Univ.,[3] Kobe Women's College,[4] Kochi Univ.,[5] National Lab. for High Energy Physics (KEK),[6] Okayama Univ. of Science,[7] Tezukayama Univ.,[8] Univ. of Alabama in Huntsville,[9] Louisiana State Univ.,[10] NASA Marshall Space Flight Center,[11] Univ. of Washington,[12] Institute of Nuclear Physics, Krakow.[13]*

0920-5632/98/$19.00 © 1998 Elsevier Science B.V. All rights reserved.
PII S0920-5632(97)00503-3

of the primary components below 100 GeV/n, ratios of secondary versus primary nuclei, and overall isotopic abundance.

There are several outstanding questions on some isotopic abundance such as ^{22}Ne, $^{25, 26}$Mg, and $^{29, 30}$Si, as well as the (C/O) ratio [3]. Multiple, specific types of the sources, such as pulsars and type-II supernova [4] and the stellar winds from Wolf-Rayet stars [3], have been introduced to account for these data; which are recently more seriously employed by Bierman [4] and others to account for the difference of helium and proton spectra indicated by the Japanese-American-Cooperative-Emulsion-Experiments (JACEE).

At higher energies above 100 TeV/n (~ 5 x 10^{15} eV for Fe), a spectral break ("Knee") has long been recognized by the Extensive Air Shower (EAS) observations, although whose data are limited to the energy flow without elemental data. Shock acceleration theories encountered a great theoretical difficulty [5] at this very energy region.

The JACEE group has carried out a series of balloon flight experiments to explore the elemental composition of these high energy nuclei directly measuring the primary charges and energies with emulsion chambers. Their high energy interactions in the detector are also measured.

This paper describes the JACEE experiments and the recent data summary on energy spectra and elemental composition up to 10^{15} eV [6]. More long duration balloon flight experiments are currently planned for the coming decade to extend the spectrum beyond the "knee".

2. INSTRUMENTS & METHODS - High Precision Emulsion Chamber

By 1996 the JACEE successfully made 14 balloon flights, including five long duration flights. Presently, data analysis is complete for the first 12 flights that include two long-duration balloon flights (LDB) from Australia to South America. The latest LDB experiments are Antarctic circumpolar flights (JACEE-10 ~ JACEE-14), whose data analyses are in progress.

In this paper, we summarize the data set from the first 12 balloon flights (up to JACEE-12). The average altitude of the level flight ranges from 3.5 g/cm^2 to 5.5 g/cm^2. On average more than 400 events per block were detected with the cascade's optical density (D_{max} for a slit size of 200 μm x 200 μm) greater than 0.2, or $\Sigma E\gamma \geq$ 1.5 TeV. The sum from all the flights amounted to 20,000 events. About 200 of the highest energy events for each block were traced for primary identification (total ≥ 8,000 events); of which, about 180 events had an energy exceeding 100 TeV. About a dozen of the high multiplicity events per block were measured for interaction studies. A total of 56 blocks of emulsion chambers was flown and the analysis on the first 40 blocks is complete for the present paper. The details of the parameters of balloon flights are listed in **Table 1.** The basic detector used in the JACEE experiments is a fine-grain emulsion chamber that has hundreds of track-sensitive emulsion plates and a three-dimensional emulsion-X-ray film calorimeter [7]. Electronic counters (such as Cherenkov detectors, proportional chambers, a gas ionization chamber and a plastic shower counter) were used in the third JACEE balloon experiment (JACEE-3).

New hybrid emulsion chambers are being built for a large area application in long-duration balloon (LDB) flights to accelerate the post-flight track analyses of a large amount of the data. Scintillation fiber hodoscopes for in-flight primary tagging and a large super-conducting magnet for track momentum measurements are tested and planned for future experiments [8]. Shown below (in **Fig.1**) are the schematic illustration of the JACEE emulsion chamber and composition of the track sensitive materials that record high energy cosmic ray nuclei, their interactions, secondary tracks, and 3-D cascade shower developments.

Table 1. JACEE Balloon Flights

Flight Number	Launch Date	Launch Site	Altitude (g/cm^2)	Flight Hours at Float	No. of Units (@Size cm x cm)
JACEE-0 Test	5/79	Sanriku	8.0	29.0	1 (40 x 50)
JACEE-1	9/79	Texas	3.7	25.2	4 (40 x 50)
JACEE-2	10/80	Texas	4.0	29.6	4 (40 x 50)
JACEE-3	6/82	Greenville	5.0	39.0	1 (50 x 50)
JACEE-4	9/83	Texas	5.0	59.5	4 (40 x 50)
JACEE-5	10/84	Texas	5.0	15.0	4 (40 x 50)
JACEE-6	5/86	Texas	4.0	30.0	4 (40 x 50)
JACEE-7 LDB	1/87	Alice Springs	5.5	150.0	3 (40 x 50)
JACEE-8 LDB	2/88	Alice Springs	5.0	120.0	3 (40 x 50)
JACEE-9	10/90	Ft. Sumner	4.0	44.0	4 (40 x 50)
JACEE10 LDB	12/90	Antarctica	3.5	204.0	2 (30 x 40)
JACEE11 LDB	12/93	Antarctica	4.5	217.0	6 (40 x 50)
JACEE12 LDB	1/94	Antarctica	5.0	212.0	6 (40 x 50)
JACEE13 LDB	12/94	Antarctica	5.0	310.0.	6 (40 x 50)
JACEE14 LDB	12/95	Antarctica	5.0	350.0	6 (40 x 50)
JACEE15 Test	9/95 Magnet	Ft. Sumner	4.5	20.	2 (40 x 50)
JACEE16 Test	9/95 Fiber	Ft. Sumner	4.0	10.	1 (40 x 50)

The bottom part of the chamber is called as the "Emulsion-Calorimeter" (EMCAL), having the vertical lead thickness (tv) of 7 - 12 radiation length (r.l.) with about 30 sampling layers of emulsion plates with x-ray films. X-ray films provide visible record of individual cascades and emulsions give a fine spatial resolution of ~ 1 micron. The 3D cascade theory for a small radius (Ne(r)) is applicable to the JACEE EMCAL. For 3D shower development (Ne (t) for r < 100 μm) EMCAL well performs a sampling calorimetry beyond the shower maximum (tv max ~ 7 - 10 r.l.) for those with energy exceeding $\Sigma E\gamma = 100$ TeV. The visible dark spots in X-ray films are useful for visual scanning and densitometry for determining the shower energy. The detection threshold energy varies with the background density, and it is typically $\Sigma E\gamma = 700$ GeV ($D_{max} = 0.1$). All the detected events are measured for zenith angle (θ), azimuth angle (φ), and optical density (D_{max}). Since the event tracing throughout hundreds of emulsion layers for each event is time consuming, only high energy events were selected for the analysis. The criteria for event selection are $D_{max} \geq 0.20$, *0.29, and 0.35* for JACEE 1 - 6 [6], JACEE 7, and JACEE 8, respectively. The zenith angle cut was also applied for the analysis. Typically, we select $\tan\theta \leq 5.0$ ($\theta \leq 79^o$) for high energy events ($D_{max} \geq 0.5$) and $\tan\theta \leq 3.0$ ($\theta \leq 72^o$) for events with $D_{max} < 0.5$. The solid angle acceptance of the chamber with these criteria is very high (3 - 3.5 sr) compared with that of a typical electronic calorimeter (~ 0.1 sr).

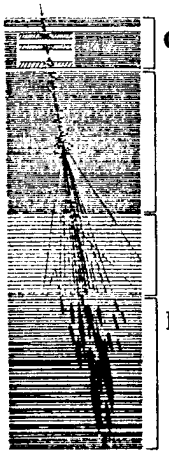

Fig. 1 JACEE Emulsion Chamber.

The energy measurements of individual events were made by the optical densitometry of X-ray films. The D_{max} value was calibrated by the electron density counting (Ne) in emulsions for the same events. The empirical formula of the shower energy for a measured value of Ne_{max} ($r > 100\mu m$) was

$$\Sigma E\gamma \ (GeV) = 10.6 \times \{(Ne_{max} - 1) \times (1 + \tan\theta)^{0.25}\}^{1.08}. \quad (1)$$

The accuracy of energy measurements was studied by using Monte Carlo simulations incorporating shower-to-shower fluctuations in sampling calorimetry. This fluctuation is naturally larger for a larger primary nucleus. Our results of overall errors are shown in **Fig. 3**, where 1σ's in the relative error ($\Delta\Sigma E\gamma$ / $\Sigma E\gamma$) are 18%, 23%, 27%, 30%, and 42% for protons, helium, C-O, Ne-S, and Fe nuclei, respectively.

These values include the fluctuation due to that of the interaction heights from event to event in the emulsion chamber. What we obtain is the $\Sigma E\gamma$ spectrum for each primary species. The primary energy (E_0) spectrum is then obtained from the observed $\Sigma E\gamma$ spectrum by using the conversion factor $C_{k\gamma}^{-1}$. The $C_{k\gamma}$ uniquely relates the primary E_0 spectrum and the $\Sigma E\gamma$ spectrum, and is defined by $C_{k\gamma} =$ $[\int k\gamma^{\beta} f(k\gamma)\, dk\gamma]^{1/\beta}$, where β denotes the primary power index and $f(k\gamma)$ is the partial (photonic) inelasticity distribution in nucleus (nucleon) - nucleus interactions. The $C_{k\gamma}$ values are different for events that interacted in the target and EMCAL. The former is about 10% smaller than the latter. The $C_{k\gamma}$'s for the target interaction events are 0.265, 0.168, 0.129, 0.115, and 0.105 for protons, helium, carbon, magnesium and iron, respectively.

The upper portion of the emulsion chamber consists of the PRIMARY MODULE and the TARGET MODULE where many emulsion plates and some CR-39 plastic detectors permit charge measurements and interaction studies. Most of CR-39 plates, however, did not give better charge resolution than the δ-ray range-spectrum measured in emulsions. **Fig. 4a** shows the charge distribution of the accelerator nuclei (^{16}O, 200 GeV/n) with various dip angles (0°, 30°, 45°, 60°, 90°) measured by CCD photometry ($\Delta Z \sim 0.6e$ for oxygen nuclei).[9] **Fig. 4b** shows the measured distribution for nuclei that were detected by cascade showers at high energies ($E > 1$ TeV/n, $\Delta Z = 0.57e$ for $Z = 6 \sim 12$).

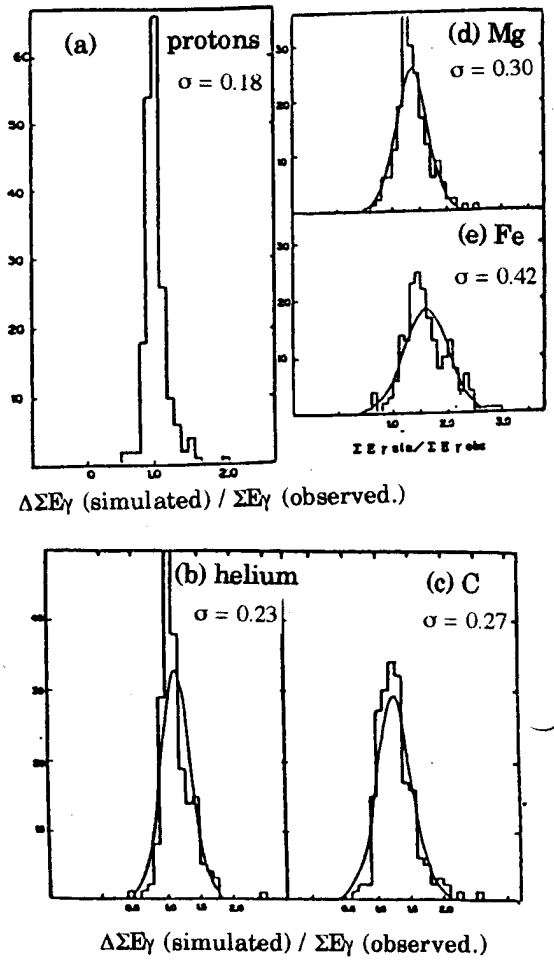

Fig. 3. Energy resolution for (a) protons, (b) helium, (c) C, (d) Mg and (e) Fe nuclei.

Tracks with small charges ($Z < 5$) were measured by grain or gap counting methods in low sensitivity emulsions (Fuji 6B) as well as in high sensitivity emulsions (Fuji 7B). The measurement accuracy was $\Delta Z = 0.2e$ for protons and helium. The discrimination of protons from helium was made with ~ 100% efficiency. Some other emulsion chamber experiments do not have this capability. JACEE's identification of protons and helium is unique at all angles, thanks to precision triangulation of the event axis by using several background nuclei for fiducials.

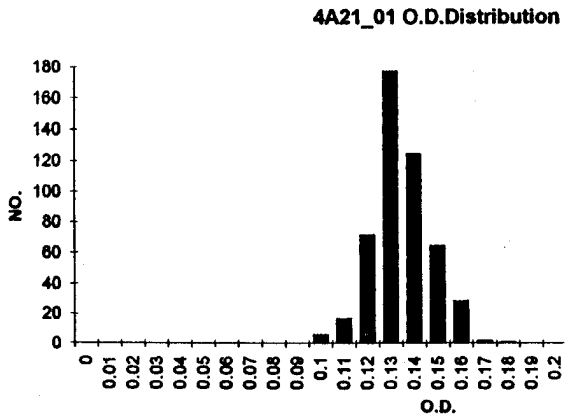

Fig. 4a. Charge resolution by track-densitometry of ^{16}O nuclei at 200 GeV/n.

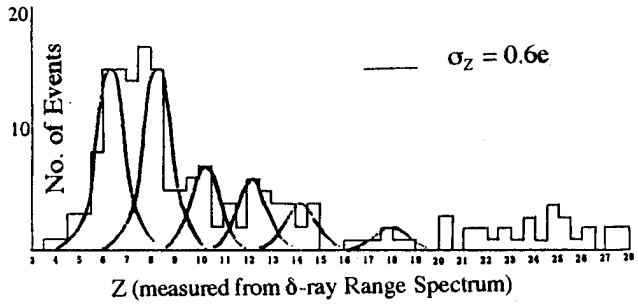

Fig. 4b. Charge resolution by δ-ray range measurements for nuclei having high D_{max}.

The error in locating the primary track in the emulsion plate was only 10 μm. There are practically no spurious background tracks with the same (θ, φ) values within this small area, and the unique identification of the primary track was accomplished even for a neutron incidence.

3. RESULTS (1) :
3.1 PROTONS AND HELIUM

Atmospheric corrections, and small intensity corrections due to finite energy resolution, were applied to the observed spectra. **Fig. 5** shows the results for protons and helium. The heium spectrum can well fit to a single power spectrum over the entire energy range of the measurement (2.5 ~ 110 TeV/n):

$$dN/dE = (7.76 \pm 0.52) \times 10^{-3} \times E^{-2.67 \pm 0.08} (m^2 \text{ sr sec TeV/n})^{-1}. \quad (2)$$

The proton spectrum shown in **Fig. 5** should further be corrected for a rising cross section by a factor of $E^{-0.03}$ to be applied to the points shown in the figure. After this correction, the Maximum Likelihood fit to proton data in the low energy region (6 ~ 40 TeV) gives

$$dN/dE = (7.49 \pm 0.20) \times 10^{-2} \times E^{-2.64 \pm 0.12}. \quad (3)$$

Protons in the entire energy range 6 ~ 300 TeV can be represented by a single power,

$$dN/dE = (1.04 \pm 0.04) \times 10^{-1} \times E^{-2.79 \pm 0.05} (m^2 \text{ sr sec TeV})^{-1}. \quad (4)$$

Two-component fit with the bending point at E ~ 50 TeV, if desired, can be:

$$dN/dE = (7.49 \pm 0.20) \times 10^{-2} E^{-2.64 \pm 0.12} \times [\theta(E - 6 \text{ TeV}) \{1 - \theta(E - 50 \text{ TeV})\}] + (6.2 \pm 0.80) \times 10^{-1} E^{-3.0 \pm 0.20} \times [\theta(E - 50 \text{ TeV})]. \quad (5)$$

Some deficiency of the proton intensity above 40 ~ 50 TeV was recognized in 1993 with the data up to JACEE-8. If it is real and of rigidity-dependent astrophysical origin, it should also be seen in helium spectrum at energies above 20 ~ 25 TeV/n. However, there were no such evidence for the helium spectrum. If instrumental artifacts such as saturation of optical density were to be blamed, the same deficiency in helium spectrum should occur at energies above 16 ~ 20 TeV. No such effects were recognized in 1993 in the observed helium spectrum. If the high energy bend in proton spectrum is due to unknown hadronic interactions, it can happen for helium at approximately the same energy per nucleon.

3.2 Exact Densitometry: corrections required for X-ray film photometry

It was recently discovered [10] that the traditional definition of D, used by all the emulsion chamber experiments including mountain-top X-ray chambers, was significantly inaccurate for high energy shower measurements. Exact corrections were applied to all the present JACEE 1- 12 data. The proton flux deficiency indicated in 1993 (Calgary) above 50 TeV is not significant with the new data summary up to the recent JACEE-12 experiment. Below we show why this photometry correction is mandated and how significant it is.

The optical densities measured in the densitometry are D_{ob} (shower + background) and D_{bg} (background), and the conventional definition [11] of the optical density of the shower (D_{sh}) is simply

$$D_{sh} = D_{ob} - D_{bg}. \tag{6}$$

This world-wide convention of eq. (6) that defines the shower density D_{sh} is, however, only approximate and valid only for low optical density measurements. It becomes increasingly inaccurate for higher energy events that have high D_{ob} and/or D_{bg} values. This is because the quasi-linear response function of the Optical Density of X-ray films gradually deviates from the linearity at very high electron densities (ρ), and which would ultimately saturate to the asymptotic density value (D_0),

$$D = D_0 \left(1 - \frac{1}{1 + \alpha\rho}\right). \tag{7}$$

High energy events that have high optical density, $D_{sh} > 2$, in high background-density exposures ($D_{bg} \geq 0.8$) are subject to corrections corresponding to the exact definition of the optical density subtraction formulae (9) shown below for the shower, D_{sh}. The electron density of the shower (ρ_{sh}) and background (ρ_{bg}) must be used in subtracting the background density from the total electron density (ρ_{ob}) observed in the X-ray films. The correct electron density and the optical density of the shower at all ranges of the optical density is :

$$\rho_{sh} \equiv \rho_{ob} - \rho_{bg}$$

$$= \frac{D_0(D_{ob} - D_{bg})}{\alpha(D_0 - D_{ob})(D_0 - D_{bg})}, \tag{8}$$

and

$$D_{sh} = D_0 \left(1 - \frac{1}{1 + \alpha\rho_{sh}}\right) = \kappa\,(D_{ob} - D_{bg}), \tag{9}$$

where

$$\kappa \equiv \left[\left(1 - \frac{D_{bg}}{D_0}\right) - \frac{D_{bg}}{D_0}\left(1 - \frac{D_{ob}}{D_0}\right)\right]^{-1}. \tag{10}$$

We note here that the exact formulae (9) should be used in any high energy densitometry experiments where the shower density (D_{sh}) and the background density (D_{bg}) are not negligibly small to use eq. (6), e.g., eq. (6) inaccurately gives $D_{sh} \sim 3.0$ for a high energy shower event of $D_{sh} = 3.5$ for a background $D_{bg} \sim 1.0$. Correspondingly, air shower (gamma family) data from all the

mountain-top experiments should receive the corrections by eq. (9). (Almost all the mountain experiments data remain uncorrected, and therefore, they could be regarded as significantly underestimating the energy ($\Sigma E\gamma$ and $E\gamma$) in any relevant data analyses.)

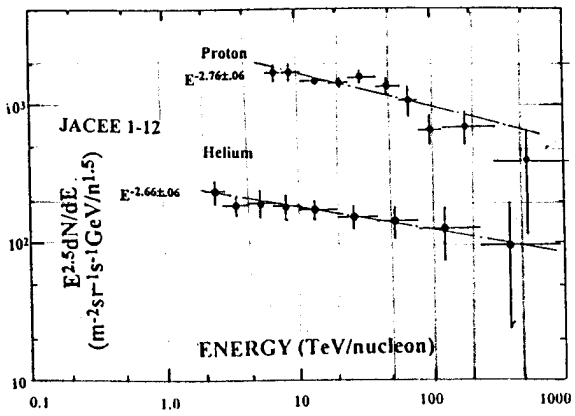

Fig. 6 Proton and helium energy spectra from the corrected JACEE 1 - 12 data.

3.3 Summary of the Proton spectrum

The flatter (-2.64) single power-law spectrum for the data points below 50 TeV, (3), is a poor fit for the data points above 50 TeV. Present data, being corrected by the proper photometric energy determination formula is quite consistent with a steeper (- 2.79) single-power law spectrum (4) in the entire energy range. The two-component spectrum (5) can fit the data, but the statistical confidence level for two-exponent spectrum is not meaningfully higher than the single power-law spectrum. The essential difference of the present data from the 1993 summary can be seen in the D→E conversion. The puzzle and question stated in 1993 paper and in the section **3.1.** in this paper regarding the proton deficiency seem to be well solved by the finding of the inappropriate D→E conversion scheme that has been conventionally used by all the emulsion chamber experiments for years. The on-going analysis of Antarctic circumpolar balloon flight series (JACEE-13 and -14) is expected to give a few times larger statistics than the present one and more definitive answer to the question on the possible steepening of the proton spectrum beyond 100 TeV could be answered soon. Further observations would be required to examine a possible "knee" of protons at higher energy. More than 30 times larger statistics than the present summary is required to examine with a sufficiently high statistical confidence to 1000 TeV regime.

$\ln \bar{E}$= 4.66 4.90 5.27 5.72

Table 2 Number of events and exposure factors for different charge groups (JACEE)

Item \ Energy Bin	38 - 55 TeV $\bar{E}$ 45.7	55 - 116 TeV 79.9	116 - 300 TeV 186.5	300 - 930 TeV 528	> 930 TeV
Protons No. of events	38	38	14	3	0
for SΩTp (m^2 sr s)	8.84×10^5	1.64×10^6	1.64×10^6	1.64×10^6	1.64×10^6
Helium No. of events	53	54	22	7	1
for SΩTp (m^2 sr s)	9.72×10^5	1.13×10^6	2.27×10^6	2.27×10^6	2.27×10^6
C - O No. of events	22	26	12	9	1
for SΩTp (m^2 sr s)	7.63×10^5	7.63×10^5	1.04×10^6	1.29×10^6	1.29×10^6
Ne - S No. of events	10	15	9	3	0
for SΩTp (m^2 sr s)	1.10×10^6	1.10×10^6	1.33×10^6	2.89×10^6	2.89×10^6
Z > 17 No. of events	6	11	9	3	2
for SΩTp (m^2 sr s)	9.20×10^5	1.11×10^6	1.35×10^6	2.92×10^6	2.92×10^6
<ln A> (A: mass No.)	1.49 ± 0.14	1.64 ± 0.11	2.11 ± 0.17	2.03 ± 0.24	2.67 ± 0.59

*S: effective area, Ω: solid angle, T: exposure time, p: Interaction probability (within the fiducial volume).

FTP	He	FTP	N	FTP	H	FTP	VH	FTP
245	53	240	22	212	10	305	6	

E	P/Z>2	δ
45.7	0.96 ± 0.22	23%
79.9	0.40 ± 0.08	20%
186	0.34 ± 0.11	32%
528	0.20 ± 0.13	65%

4. RESULTS (2): NUCLEI

The energy spectrum (per nucleon) for nuclei heavier than helium are shown in **Fig. 7.** Compared in the figure are lower energy summary of the CRN and SOKOL spacecraft experiments (S. Swordy [12]). Uncertainties for the different experimental conditions and the limited statistics would discourage quantitative comparison of them. Nevertheless, overall comparison suggests that the heavy nuclei's spectra are harder than those of protons and helium spectra. All these three experiments are different in instrumental principles and methods. Any relative systematic bias, if any, can reduce the validity of such a comparison. To avoid unknown influence of any systematic errors, we confine our discussions to the abundance data within the JACEE experiments only.

Table 2 shows the number of events at five energy bins, where relative abundance of different charge groups can be seen at different energy. It is evident from this table that the average mass (< ln A >) is increasing with increasing energy.

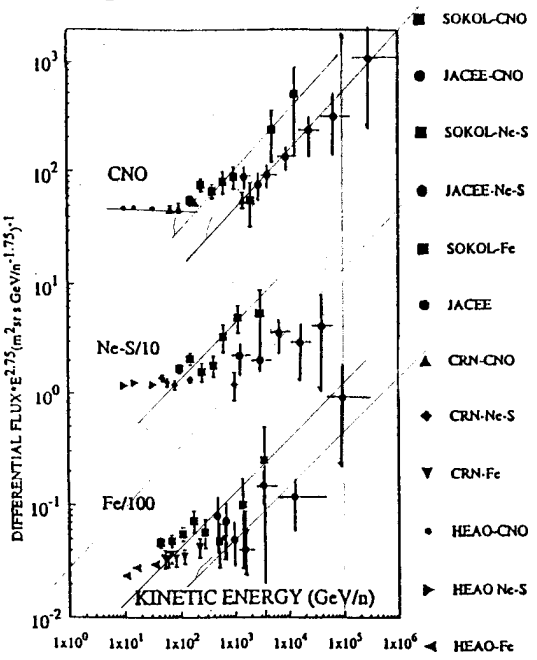

Fig. 7 Differential energy spectrum for Z > 5 nuclei (energy per nucleon).

At the highest energies (300 - 930 TeV, with the median of 500 TeV) the abundance of (C ~ Fe) is 60 ± 20%, which is 1.7 times increase from that of 36.4 ± 7.5% at 45 TeV (38 ~ 55 TeV). The 1.7 times larger value is only a 1.5σ argument. Therefore, the result on heavy nuclei dominance still requires a larger statistics' analysis for a conclusive judgment. The all-particle spectrum and the energy spectra per nucleus for each charge group are shown in **Fig. 8.** It is noted here that the JACEE result on the all-particle spectrum is very similar to that of old PROTON satellite results [13], but neither of them reached the very "knee" of the AS spectrum [14]. Both data smoothly connect to the AS data.

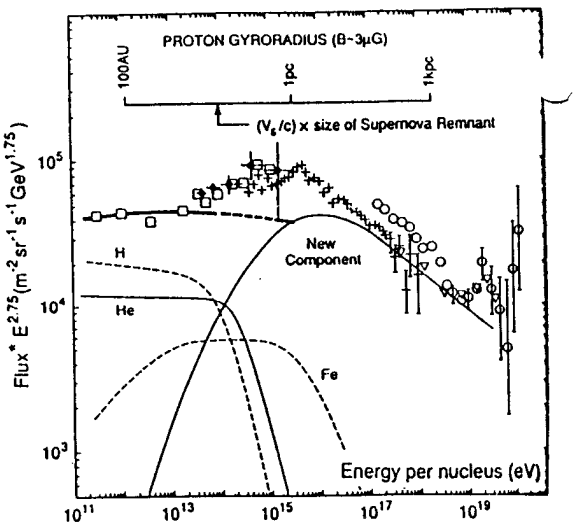

Fig. 8. All-particle spectrum (E per nucleus)

5. RESULTS (3): L/M RATIO

The Light nuclei (Li + Be + B) vs Medium primary nuclei (C + O) is a good measure to evaluate the material path length of cosmic rays after propagating in the galaxy. This value in this experiment was 0.065 ± 0.03(at the median energy of 7 TeV/n. It clearly contradicts with the predicted values (> 0.2 for the Closed Galaxy Model and agrees very well with the Nested Leaky Box Model while much smaller values are expected fo

the Leaky Box Model. The analysis, however, has an uncertainty of about 1 g/cm^2 in evaluating the background, and the observed ratio does not necessarily preclude the Leaky Box Model. **Fig. 9** compares the high energy JACEE data with the low energy data and these three major models.

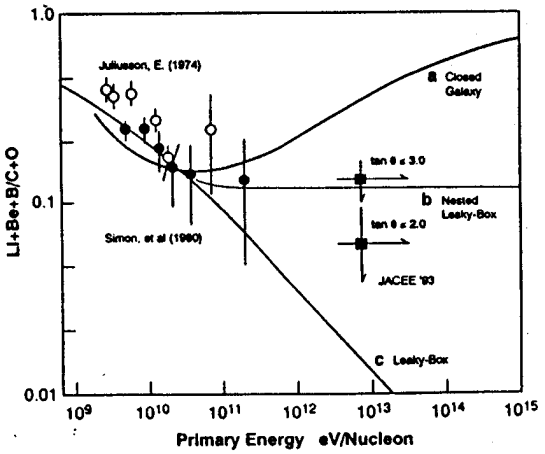

Fig. 9 L/M ratio.

6. DISCUSSIONS

Very high energy composition data on cosmic ray elements suggest some deviation from those well known for years at lower energies (E < 1 TeV/n). Notable points of "anomalies" in cosmic ray data above 1 TeV/n are:

1) Difference in spectral index of protons and helium to 0.1 ± 0.06 from the low energy to high energy up to 50 TeV/n (JACEE and Chicago).

2) Suspected early steepening of proton spectrum at higher energies before the "knee", although there are no compelling evidence or indications for protons or corresponding steepening for Helium spectrum up to 100 TeV/n (JACEE).

3) Hard spectra of C - O components with the spectral index of - 2.46 ± 0.16 (JACEE & Maryland).

4) Gradual increase of the average mass number toward the "knee" (HEAO, CRN, and JACEE) and its gradual decrease beyond the "knee" to 10 ^{18} eV (Fly's Eye).

5) Possible increase of Ar and Ca components above 500 GeV/n (HEAO C3).

6) Possible decrease of Si component above 500 GeV/n (Chicago CRN and Sanriku).

Some understanding of these data have been provided by the latest model of Biermann et al, who considered the two components of cosmic rays up to the "knee"; namely, (I) SN shock wave acceleration of interstellar medium to account for Hydrogen up to 30 GeV and the similarity of the low energy composition with the FIP-dependent Solar Abundance; (II) SN-II explosion into stellar winds of massive stars, to account for high energy He and nuclei. Here, however, additional remarks are due to a possible decrease of Si, and possible increase of Ar, Ca and sub-Fe components, in addition to the hard spectrum of C-O components.

If all these data were correct, as well as those of protons and Helium, the available data would favor the second component scenario from SN-II. Should the second component at high energies contain not only the elements of the stellar winds but also those of SN-II ejecta, we might be led to consider either pulsar winds and direct DC acceleration or shock acceleration of the SN-II ejecta in the association of massive stars. Explosive neutron process of the Si layer that produces S, Ar, Ca would have to be taken into account of the analysis for high energy medium-heavy abundance.

Thus, the question of the second component and the details of the composition change at around the "knee" might shed light on the origin of cosmic rays in more concrete way than before.

7. CONCLUSIONS

High energy cosmic rays have been observed in the energy region 10 TeV -

1000 TeV by the JACEE balloon flight experiments. The data used in the analysis are from 580 m^2· hour exposure. The latest Antarctic balloon flights increased the exposure to 1,212 m^2.hour.

The all-particle spectrum close to the "knee" region indicates a flatter spectrum than that of protons, consistent with the PROTON satellite data. Protons in the energy range 6 TeV - 350 TeV is still consistent with a single-power law with a slope of - 2.79 ± 0.05. Helium fits very well to a single-power law spectrum in the energy region 2.5 - 200 TeV/n with a power index of - 2.66 ± 0.06. A possible steepening of the proton spectrum is an interesting question, but a definitive answer must await higher statistics' studies.

Medium nuclei (C ~ O), medium heavy nuclei (Si ~ S) and iron group nuclei (+ sub-iron, Z ≥18) indicated generally flatter spectra than the proton spectrum, suggesting heavy dominance toward the "knee" region. The L/M ratio at median energy of 7 TeV/n indicated a small value (0.065 ± 0.030), clearly excluding a possibility of the Closed Galaxy Model or large-scale reacceleration models, while supporting Leaky or Nested Leaky Box models. The major elements' composition data at above 10 TeV/n indicate substantial deviations from the simple extrapolation of the low energy spectra and composition. Further data from large-scale experiments are imperative to go beyond any of the current, qualitative arguments and modeling on the origin of high energy nuclear elements.

The JACEE experiments are supported in U.S. by the Department of Energy, National Aeronautics and Space Administration, National Science Foundation; and in Japan, by Kashima Foundation, Ministry of Education, and Yamada Science Foundation. Successful balloon flights were provided by the U.S. National Scientific Balloon Facility.

REFERENCES

1. J.J. Engelmann et al., 18th ICRC Bangalore, 2, 17 (1983); W.R. Binns et al. Ap. J. 324, 1106 (1988); D. Müller et al. Ap. J. 374, 356 (1991).
2. J.F. Ormes and P.S. Freier, Ap. J. 222 471 (1978); C.J. Cesarsky, Ann. Rev. Astr Ap., 18, 289 (1980); E. Juliusson, P. Meye and D. Müller, Phys. Rev. Lett. 29, 44 (1972); W.R. Webber et al., Nature Phys Sci. 241, 96 (1973); J.F. Ormes and V.K Barasubrahmanyan, Nature Phys. Sci. 241 95 (1973).
3. W. R. Webber et al., 19th ICCR, 2, 8 (1985); J. P. Meyer, Ap. J. Supple. 57 (1985).
4. S. Karakura, J. L. Osborne and A. W Wolfendale, J. Phys. A7, 437 (1974); R Leinemann and K. O. Thielheim, Ap. Supple. 66, 19 (1988); Y. Takahashi et al. Nature 321, 839 (1986); P. Bierman Astron. Ap., 1993; 23rd ICRC, Calgary Invited Talk Vol., 45 (1994)
5. P. O. Lagage and C.J. Cesarsky, Astron & Astrophys., 125, 249 (1983); R. D Blandford and D. Eichler, Phys. Rep. 154, (1987); W. I. Axford, GOAL Workshop Calgary, 1993.
6. K. Asakimori et al., 23rd ICRC, 2, 21 25 (1993); T. H. Burnett et al., Ap J. 349 25 (1990); 24th ICRC, Rome, (1995).
7. T. H. Burnett et al., Nucl. Instr. Method A251, 583 (1986); T. A. Parnell et al., Adv Sp. Res. 9, 45 (1988).
8. T. A. Parnell et al., 23rd ICRC, Calgary 2, 567; R. J. Wilkes et al., 4, 708 (1993).
9. B.L. Dong and Y. Takahashi, U o Alabama, 1996 (unpublished).
10. Y. Takahashi, ECT Report, 1995, 1996
11. I. Ohta et al., NIM, 161, 35 (1979).
12. S. Swordy, Proc. 23rd ICRC, Rapporteu Volume, 243 (1994).
13. N. L. Grigorov et al., Proc. 12th ICRC Hobart, 5, 1746 (1971).
14. EAS Summary, see: A. M. Hillas, Ann Rev. Astro. Ap., 22, 425 (1984).